

Urban Effects on Summer Monsoon Convection in Phoenix, Arizona (USA):

A Model Case Study of Aug. 2-3, 2005

Susanne Grossman-Clarke^{1,2}, Joseph A. Zehnder³, Christopher L. Castro⁴, Yubao Liu⁵ and
William Cassell⁴

(1) Global Institute of Sustainability, Arizona State University, Tempe, AZ, USA

(2) Potsdam-Institute for Climate Impact Research, Potsdam, Germany

(3) Department of Atmospheric Sciences, Creighton University, Omaha, NE

(4) Department of Atmospheric Sciences, University of Arizona, Tucson, AZ

(5) Research Applications Laboratory, NCAR, Boulder, CO

19 April 2011

Corresponding Author

Dr. Susanne Grossman-Clarke

Arizona State University

Global Institute of Sustainability

PO Box 875402

Tempe, AZ 85287-5402

Email: sg.clarke@asu.edu

Abstract

The Weather Research and Forecasting Model (WRF) was used to simulate a typical North American Monsoon thunderstorm event on 2-3 August 2005 in Phoenix, Arizona (USA). Using a factor sensitivity analysis, the impact of urban physical characteristics that may affect thunderstorm development were investigated, including increased surface roughness, agricultural and landscape irrigation, increased heat storage and anthropogenic heating. WRF is able to reproduce the timing and propagation of the convective event reasonably well. In agreement with the observed precipitation pattern, urban physical effects led to a reduction of simulated rainfall over Phoenix and enhanced precipitation on the northern fringe of the city. A reduction of afternoon urban sensible heat fluxes, H , clearly has the most pronounced effect on precipitation by causing a complex response in the storm propagation from elevated terrain into Phoenix and changing locations of convergence zones. The non-linear interactions of urban characteristics affect precipitation strongly also but their superposition cancels much of the impact. This case study suggests that the impact of urbanization on thunderstorms in the semi-arid and mountainous southwest U.S. may be markedly different than in more humid climates due to a reduction of urban afternoon H in comparison to the rural surroundings.

1. Introduction

Observations, experimental and modeling studies showed that rainfall and convective activity are enhanced in urban regions located in mid-latitude humid climates of the U.S. Examples include New York City (Bornstein and LeRoy 1990); Atlanta, Georgia (Bornstein and Lin 2000, Shem and Shepherd 2009); St. Louis, Missouri (Changnon 1981, Rozoff *et al.* 2003); Chicago, Illinois (Changnon 2001); Houston, Texas (Orville *et al.* 2000; Burian and Shepherd 2005, Shepherd *et al.* 2010) and Oklahoma City (Hand and Shepherd 2008). The physical processes responsible for the increase in precipitation have not been fully identified (Cotton and Pielke 2007) but mesoscale meteorological model simulations show that higher sensible heat fluxes over the urban compared to surrounding rural areas lead to deeper and drier planetary boundary layers (PBL), causing low-level convergence that is favorable for generating cumulonimbus clouds and initiating convection downwind of the city (Bornstein and Lin 2000, Rozoff *et al.* 2003, Cotton and Pielke 2007). Another possible mechanism affecting precipitation is an increase in surface momentum flux due to the presence of buildings that causes air to diverge around the urban core and converge downwind. Urban aerosols can also have significant impacts on microphysical processes in clouds and enhance or suppress precipitation depending on cloud type, seasonality, climate regime or orography of the urban region (Shepherd 2005).

The focus of the present study is on the Phoenix metropolitan area (Fig. 1a), located in the Salt River Valley, at an elevation of 335m and with elevated terrain to the north and northeast of the city (Fig. 1b). Summer weather in Phoenix is influenced by the North American Monsoon (NAM), which results in a maximum of convective activity and rainfall in July and August (Adams and Comrie 1997). On most days conditions for thunderstorm development are marginal due to a lack of both low-level moisture and upper-level instability (Maddox *et al.* 1995) and precipitation in Phoenix occurs in just a few isolated “burst”

periods of organized convection. When monsoon thunderstorms do occur, there are several key factors typically present. The upper-level subtropical high pressure moves to the north and east of central Arizona and the region is under the influence of moist easterly flow at upper-levels (e.g. Bryson and Lowry, 1955). The presence of upper-level instability and wind shear caused by a synoptic-scale disturbance, such as an inverted trough (e.g. Bieda et al. 2009), and/or a surge of low-level moisture (e.g. Hales, 1972) is additionally required for the development of thunderstorms. Given these preconditions, convection typically develops over the mountains to the north and east of Phoenix. Thunderstorms organize and move westward into the city and the low-deserts of southwest Arizona via discontinuous propagation. New convection is initiated along the outflow boundaries from existing cells (Smith and Gall, 1989). The convective maxima occurs in the late evening hours likely due to the destabilization of the mid-level troposphere by westward advection of cooled air from cumulus areas in the adjacent higher terrain (Hales 1977, Balling and Brazel 1987a, Svoma 2010).

It is of great interest to study to what extent the Phoenix metropolitan area is influencing the propagation of thunderstorms through the region. Previous statistical analyses of historical observations suggest that the city is indeed influencing monsoon rainfall. Balling and Brazel (1987b) analyzed rain gauge data at Phoenix Sky Harbor Airport and concluded that rainfall events between midnight and noon declined during the years 1970-1985 in comparison to the period 1954-1969. The later period was characterized by rapid population growth and an increase in nighttime air temperatures. Based on the analysis of 1950-2000 precipitation data from surface weather stations Diem and Brown (2003) found that precipitation amounts are higher in the Lower Verde River Basin, ~30-50 km northeast of Phoenix, compared to the neighboring valleys. They argue that moisture from agricultural and landscape irrigation is advected to that region. For the same area Shepherd (2006) also

showed a statistically significant increase in mean precipitation of $\sim 12\%$ from the pre-urban (1895-1949) to the post-urban (1950-2003) period. Shepherd (2006) assumes that the urban heat island and irrigation lead to advection of moisture into this preferred convergence zone.

These studies are statistical analyses of rainfall, hence the mechanisms leading to the observed precipitation patterns remain unclear. There have been no mesoscale modeling studies carried out to investigate the mechanisms by which Phoenix or other cities in the southwest U.S. might potentially influence thunderstorm development. Therefore in this study the Weather Research and Forecasting (WRF) model (Skamarock et al. 2005) along with the Noah urban canopy model (Noah UCM; Kusaka and Kimura 2004) is applied for a NAM thunderstorm event on 2-3 August 2005 in Phoenix, with the goal to analyze mechanisms underlying urban modifications of the convective event. Studying urban effects on monsoon convective activity in central Arizona using mesoscale models is inherently challenging, since it is necessary to capture convective initiation over the higher terrain (Bright and Mullen 2002), the evolution of the urban PBL and the thermal mesoscale circulations that interact with the thunderstorm outflow propagating from the elevated terrain.

Another challenge involves assessing contributions of the various forcing factors. Rozoff et al. (2003) applied the Stein and Alpert (1993) factor separation method to investigate effects of topography, urban heat and momentum fluxes on convection in St. Louis. In a similar manner, we apply the factor separation approach to study the contribution of urban modifications including roughness, agricultural and landscaping irrigation, heat storage, anthropogenic heating, albedo and emissivity to the thunderstorms on 2-3 August 2005 in Phoenix. In the following sections we firstly give an overview of the thunderstorm event (section 2a), then WRF model configuration (section 2b) and the scenario simulations required by the Stein-Alpert method (section 2c). WRF's ability to simulate the thunderstorm

event with sufficient accuracy is analyzed in section 3, along with the analysis of the Stein-Alpert scenario simulations. The fourth and final section summarizes the important results.

2. Data, model and analysis methods

a. Convective event

On August 2-3, 2005 typical severe thunderstorms occurred in the Phoenix region. The requisite conditions for organized convection in the low deserts of Arizona described above were present. The conditions generally fit the Type I classification of severe thunderstorms in Arizona proposed by Maddox et al. (1995). Figure 2a shows the 500 hPa height at 00 UTC 3 August 2005, obtained from the National Center for Environmental Prediction (NCEP) Final Operational Global Analysis (FNL) gridded data (a 1° resolution every 6 h). The upper-level subtropical high was located over the central U.S., northeast of its climatological position at this time of year over the Four Corners region, providing favorable easterly winds to push storms off the terrain (Fig. 1b). Water vapor imagery (not shown) indicated the presence of an upper-level inverted trough over northern Mexico, which provided the diffluence and forced lifting to the north and west over central Arizona.

Heinselman and Schultz (2006) describe a classification of precipitation regimes in Arizona based on 500 hPa heights along with the water vapor and precipitation distribution. The scheme is based on the assumption that the NAM is regulated by the 500 hPa flow with variations depending on the location of the North Pacific trough and the subtropical high that regulate the location of the meridional moisture axis. The storm event analyzed in this study corresponds closely with their Central-Eastern Mountain and Sonoran Regime. A meridional axis of moist air is centered over the border of Arizona and New Mexico (Fig. 2b) with the ridge being shifted slightly northward and its axis tilted toward the northwest, providing middle level tropospheric moisture in the region.

The Phoenix sounding with vertical profiles of air temperature, dew point temperature, wind speed and direction at 00 and 12 UTC on 3 August 2005 is shown in Fig. 3a and 3b. Winds are easterly between 300 and 600 hPa, consistent with the 500 hPa heights in Fig. 2a. Below 850-mb the low-level winds are westerly, with a relatively high dewpoint of 15 °C and 14 °C, indicative of a surge of moisture from the Gulf of California. Smith and Gall (1988) described the propagation of tropical squall lines associated with the NAM. The low level westerlies associated with the gulf surge force moist, unstable boundary layer air up along the gust front associated with the downdraft of an existing cell. This causes a discontinuous propagation of the cells at a speed that is larger than the flow at any level. Smith and Gall also showed that a dry layer at middle levels aids in the tropical squall line propagation through downdraft development associated with mid-level entrainment and evaporative cooling. There is evidence of a dry layer between 400-600 hPa in the 00 UTC sounding (Fig. 3a), while the 12 UTC sounding (Fig. 3b) shows the classic convectively modified “onion” sounding (Zipser 1977) due to PBL cooling and moistening by downdrafts. There is evidence of middle level moistening as a saturated layer appears near 500 hPa.

Figure 4a shows hourly accumulated precipitation amounts, P_{acc} , from the NCEP Stage IV precipitation analyses (based on NEXRAD and rain gage measurements) over Arizona for 02 August 2005 1100 LST (1800 UTC) to 03 August 2005 0500 LST. Convection began over the elevated terrain about 100 km to the northeast and east of the city at about 11 LST; the storm activities over the mountainous regions continued in early afternoon and moved to lower elevations by mid-afternoon; widespread storms over the Sonoran Desert and propagation towards the Phoenix region is visible between 1600 and 2000 LST with the heaviest rains occurring in the urban area between 2000 and 2300 LST. Around the National Weather Service station at Sky Harbor Airport (Fig.1a) P_{acc} was observed to be 25-50 mm. At 2200 LST widespread thunderstorms occurred in central

Arizona with the leading edge of the convection having passed Phoenix towards the northwest by 0300 LST. Damage reports from the National Weather Service, of this event include a major dust storm, golf-ball size hail, damaging winds, and urban flooding.

b. Numerical simulations

A one-way nested 24-hour WRF (3.0.1.1) model run with three domains and resolutions of 30, 10 and 2.5 km, respectively, was performed (Fig. 5) starting on 2 August 2005 12 UTC. The area included in the outer domain corresponds with recommendations by the “North American Monsoon Experiment” study (<http://www.eol.ucar.edu/projects/name/>). The smallest domain covers Arizona, northwest Mexico, and the entire Gulf of California in order to enable WRF to capture the Gulf surge.

In the simulations 37 vertical levels were used. NCEP FNL data were interpolated to provide initial and 3 hourly lateral boundary conditions for the WRF simulations. PBL processes were included via the Mellor-Yamada-Janjic scheme (Janjic 2002); microphysics through the Lin scheme (Lin et al. 1983, Chen and Sun 2002) that considers ice, snow and graupel processes and is suitable for real-data high-resolution simulations; radiation processes through the Community Atmosphere Model’s radiation scheme (Collins et al. 2004); and natural land surface processes by the Noah land surface model (Noah LSM; Chen et al. 1997). Convection for the outer domains was parameterized by the Kain-Fritsch scheme (Kain 2004).

In WRF, the Noah UCM and LSM are applied to the fraction of a model grid cell with built and natural surfaces, respectively. The Noah UCM considers urban geometry in the surface energy balance and momentum flux calculations (Chen et al. 2011). A multi-layer heat conductivity equation is solved for roof, wall, and road temperature profiles. Sensible heat fluxes from the respective surfaces are aggregated into the total flux H_{urban} . An anthropogenic heat flux, Q_A , can be activated which is added to the H_{urban} . Appropriate Q_A for

Phoenix were derived by the Sailor and Lu (2004) method. Maximum Q_A occur during the evening rush hour (LST 1700) and amount to $\sim 30W m^{-2}$ with slight variation between urban land use / land cover (LULC) classes (Grossman-Clarke et al. 2005). Three urban LULC classes are included in WRF for Phoenix: commercial/industrial, mesic residential and xeric residential, which are distinguished by the fractional cover of built, vegetation and soil surfaces, building heights, roof and road widths (Grossman-Clarke et al. 2010). Landsat based LULC data for 2005 (Fig.1a) were derived using the procedure of Stefanov et al. (2001).

In order to sustain landscape vegetation and agricultural productivity in the Phoenix region, irrigation is necessary all year around. The Noah LSM does not account for irrigation but assumes soil moisture contents as obtained from WRF's initial conditions. The preferred irrigation practice for urban vegetation is drip irrigation over an extended period of time (Martin et al. 2003). This technique ensures sufficient water in the root zone for plant transpiration, but soil surfaces in between plants are usually not irrigated resulting in low soil evaporation. In order to account for the irrigation in WRF, the initial soil moisture content in the urban area was increased for the sub-surface layers but not for the top soil layer. For the usually flood-irrigated agricultural LULC the soil moisture content was increased for all soil levels.

c. Stein-Alpert sensitivity analysis

There are a number of possible mechanisms which may affect thunderstorm development in this case. The increased surface roughness, $z_{0,urban}$, might slow down thunderstorm outflows and suppress the discrete propagation of thunderstorms into the region (Smith and Gall 1988). It might also inhibit the balanced basin scale flow, resulting in a convergence zone that flanks the urban area, creating convection outside the urban area.

Evapotranspiration from extended areas of irrigated vegetation may increase the convective available potential energy (CAPE) by moistening the PBL, while reduced daytime H_{urban} may have the opposite effect on CAPE.

The Stein and Alpert (1993) method allows to isolate the model response for a physical field, f , to individual processes and their non-linear interactions (factors). Therefore f is approximated by means of a Taylor series around a control simulation f_0 in which all factors are excluded. In the case of three factors, as considered in this study, f is given by:

$$f = f_0 + \sum_{i=1}^3 \Delta f_i + \sum_{i=1}^3 \Delta f_{ij} + \Delta f_{ijk}$$

with addends Δf_i , Δf_{ij} and Δf_{ijk} being the contributions of individual factors and their combinations. Eight scenario simulations are necessary which result from each factor being modified to its urban or non-urban (rural) value combined with the urban/rural values of the other factors (Table 1). The urban factors and their contributions to P_{acc} considered here are: (1) roughness as influencing momentum fluxes, τ_{urban} ; (2) heat storage, anthropogenic heating, surface albedo and emissivity as they affect H_{urban} ; and (3) irrigation and vegetation characteristics influencing latent heat fluxes, λE_{urban} .

It is impossible to simultaneously simulate λE_{rural} and H_{urban} for Phoenix since for the correct simulation of the latter it is necessary to apply WRF's USGS LULC category 5 "cropland/grassland mosaic", while USGS LULC category 8 "shrubland" represents the native desert vegetation. This reflects the fact that non-native plant species with different physiological characteristics are used predominantly in landscaping in Phoenix. Therefore, the fully urbanized WRF was applied in order to obtain H_{urban} , while λE_{urban} (including the irrigated agricultural areas) was replaced with typical values of λE_{rural} that were obtained from S_l described below. The eight scenarios are as follows:

(1) S_{rural} resulting in simulated meteorological fields f_0 : all urban effects are excluded from the simulations. Urban and irrigated agricultural LULC is replaced with characteristics of the native desert vegetation leading to fluxes τ_{rural} , H_{rural} and λE_{rural} .

(2) S_1 resulting in f_1 : $z_{0,urban}$ is used to calculate the surface exchange coefficients for momentum resulting in τ_{urban} , while $z_{0,rural}$ is applied to give the rural values H_{rural} and λE_{rural} ;

(3) S_2 resulting in f_2 : H_{urban} was simulated, while τ_{rural} and λE_{rural} were maintained. The rural surface exchange coefficient for momentum was used in the calculations of τ_{rural} .

(4) S_3 resulting in f_3 : τ and H are maintained at their rural values by running WRF as for S_1 , however with λE_{rural} replaced with typical λE_{urban} values for the urban and irrigated agricultural LULC.

(5) S_{12} resulting in f_{12} : τ_{urban} and H_{urban} are obtained by applying WRF as in S_2 , while λE_{urban} (including the irrigated agricultural areas) was replaced with typical values of the desert category, λE_{rural} , that were obtained from S_1 .

(6) S_{13} resulting in f_{13} : τ_{urban} , H_{rural} and λE_{urban} are obtained by applying WRF as in S_1 , however the urban surface momentum exchange coefficient is used in the calculations of τ_{urban} . λE_{rural} is replaced with typical λE_{urban} values for the urban and irrigated agriculture LULC.

(7) S_{23} resulting in f_{23} : the fully urbanized WRF is applied to give H_{urban} and λE_{urban} , however the rural surface momentum exchange coefficient is used in the calculations of τ_{rural} .

(8) S_{urban} resulting in f_{123} : the fully urbanized WRF is applied to give H_{urban} , λE_{urban} and τ_{urban} , H_{urban} and λE_{urban} .

Based on these scenario simulations, fields Δf_i that express the contribution of each of the factors (1) to (3) and their interactions to the simulated difference fields obtained from S_{urban} minus S_{rural} can be determined (Table 2).

3. Results and Discussion

a. Model validation

A control simulation for the event was produced to examine simulated precipitation location and timing. Fig. 4 shows the hourly NCEP precipitation analysis and the simulated accumulated rainfall on the finest grid (d03) from 1100 to 1800 LST 2 August 2005 (Fig. 4a) and 1900 LST 2 August 2005 to 0100 LST 3 August 2005 (Fig. 4b). WRF captures the initiation of convection over the Mogollon Rim and northern Mexico at about 1100 LST as well as the storm development over the mountainous regions that continued in the early afternoon. Storm movement to lower elevations began by mid-afternoon in both the observations and simulations. However, in WRF the propagation of widespread storms from southeastern Arizona and from the northeastern mountains towards Phoenix was faster than observed. The model storms developed in the Phoenix region between 1700 and 2100 LST, about three hours before they were observed by the NEXRAD radar (between 2000 and 23 LST). After the precipitation moved through the urban area, no significant night time rains were simulated, while light rains ($< 5 \text{ mm}\cdot\text{h}^{-1}$) were observed in the Phoenix region until 0500 LST 3 August 2005. This is likely due to WRF not being able to properly represent upper level stratiform rain. The maximum observed and simulated hourly precipitation amounts are comparable, on an order of $25 - 50 \text{ mm}\cdot\text{h}^{-1}$.

The observed and simulated temperature profiles in Phoenix at 1100 and 1700 LST on 2 August 2005 (Fig. 6) show a good agreement. Warming of the atmosphere occurred between 1100 and 1700 LST with near-surface temperatures peaking at $\sim 40 \text{ }^\circ\text{C}$. The profiles of dew point temperatures, T_{dew} , indicate comparable levels of moisture for observations and simulations up to 800 hPa, although the simulated T_{dew} were higher than observed between 700 hPa and 400 hPa. This might be caused by the early onset of thunderstorm activity in the

simulations. A sharp decrease in moisture at 650 hPa was visible in the observations while a more gradual change was simulated. Both the observed and simulated soundings show easterly winds between 400 and 800 hPa. At 1100 LST the observed winds are westerly below 850 hPa, indicating that the reversal in flow direction from the nighttime easterly/northeasterly down-valley winds that originate on the large-scale terrain to the north and northeast, to the predominantly westerly/southwesterly daytime anabatic flow had occurred in the region. In the simulations the winds were still southeasterly below 850 hPa and turned westerly/northwesterly by 1300 LST. Simulated and observed winds were westerly below 800 hPa at 1700 LST.

Despite the challenges, the results demonstrate that WRF is able to produce the basic features of the event, in terms of the approximate timing in the evening hours, westward propagation of the thunderstorm into the Phoenix valley, precipitation amounts, and low-level moisture transport necessary for storm development.

b. Differences between urban and rural LULC scenarios

Surface divergence, div_{surf} , and 10m wind fields are shown prior to the thunderstorm development in the city at 1300, 1500 and 1600 LST, 02 August 2005 in Fig. 7a and b for S_{urban} and S_{rural} , respectively. Convergence in the div_{surf} fields illustrates the propagation of thunderstorms from the Mogollon Rim to lower elevations. Wind fields for 1300 LST indicate that the reversal in flow direction from the nighttime northeasterly to the southwesterly/westerly daytime upslope flow had established by that time. The upslope flow converged with outflow from thunderstorms that occurred in the northern mountains ($div_{surf} \sim -0.0002 \text{ s}^{-1}$). At 1500 LST, within the urban area, winds were light, but more pronounced northwesterly and slightly higher in S_{rural} than in S_{urban} ($\sim 3\text{-}4 \text{ m s}^{-1}$ vs. $2\text{-}3 \text{ m s}^{-1}$). At 1600 LST cooling of the mountains by convective activity modified the pressure gradient such that

the surface winds in the urban area became northwesterly instead of westerly for S_{rural} (Fig. 7b), while winds were westerly for S_{urban} (Fig. 7a).

Figures 8a and 8b show enlarged views of div_{surf} for Phoenix that clearly illustrate different locations of convergence zones relative to the city boundaries for S_{urban} and S_{rural} . The outflow of convection in the mountains converges with the westerly upslope flow closer to the city in S_{rural} with $div_{surf} \sim -0.0001 \text{ s}^{-1}$ for both scenarios (Fig. 8, 1500 LST). Areas of elevated CAPE correspond with the convergence zones and are therefore located further north, i.e. outside and at/within the city boundaries for S_{urban} and S_{rural} , respectively. CAPE values are $1600 - 1800 \text{ J kg}^{-1}$ with values being slightly higher in the S_{rural} scenario (not shown). Convergence of outflow of an initial urban storm in the McDowell Mountains (cp. Fig. 1b) appeared at the northern urban fringe for S_{urban} and at the boundaries of the northeastern part of the city for S_{rural} (Figs. 8, 1600 LST). In S_{urban} , at ~ 1700 LST (Fig. 8a) an area of convergence and elevated CAPE (not shown) occurred near the northern fringe, west of the McDowell Mountains. In contrast, in S_{rural} convergence zones are clearly located within the urban area at that time (Fig. 8a).

The half-hourly accumulated precipitation, P_{acc} , between 1600 LST and 1830 LST, 02 August 2005 for the scenarios S_{urban} and S_{rural} are given in Fig. 9. For both scenarios convection in the urban area starts with a thunderstorm in the McDowell Mountains (cp. Fig. 1b) near the northern fringe at 1600 LST. Subsequently, storms develop in the convergence areas along the northeastern fringe of the city and outside the eastern fringe for S_{urban} and along the northeastern fringe for S_{rural} (Fig. 9, 1630 and 1700 LST). In S_{urban} , at ~ 1730 LST (Fig. 9a), the storm expanded from the northeastern to the northern fringe, west of the McDowell Mountains and propagated west within the next 90 minutes. Smaller cells also developed in the central and eastern parts of the urban area at 1730 LST. Meanwhile, in S_{rural} two major cells developed over the central and eastern parts of the city at 1730 LST and

moved southwestward between 1730 LST and 1830 LST (Fig. 9b). The organized storms propagating toward northwest from southeastern Arizona reach the urban area at ~ 1700 LST and pass closer to the southern fringe in S_{rural} (Fig. 9b). The storm system has passed the urban area by ~ 2000 LST (Fig. 4b).

Figures 10a-c show 24-hour P_{acc} based on the NCEP precipitation analysis, the simulations for S_{urban} and S_{rural} and a difference plot (S_{urban} minus S_{rural}) for 0500 LST, 3 August 2005. P_{acc} for the two scenarios exhibits differences in and surrounding the urban area, with the storm being located further north for S_{urban} , resulting in less precipitation in the urban center. This agrees better with the observed P_{acc} distribution, i.e. precipitation is larger in the urban fringe areas than within the city. For both scenarios, P_{acc} is overestimated to the northwest of the city. For S_{rural} , P_{acc} is higher southwest and lower to the northwest of the urban area with differences of ~ 40 -50 mm. Figure 10 also indicates an increase in P_{acc} for S_{urban} to the northeast of the city near the Lower Verde River Basin region ($\sim 33^{\circ}50'N$; $112^{\circ}30'W$), which is consistent with Diem and Brown (2003) and Shepherd (2006) who found elevated precipitation amounts compared with neighboring valleys and a statistically significant precipitation increase from the pre-urban to the post-urban period (cp. Section 1), respectively.

The difference fields (S_{urban} minus S_{rural}) in H and λE , PBL heights, and CAPE at 1300 LST, 2 August 2005 are given in Fig. 11a-d. The simulated H are ~ 30 $W m^{-2}$ higher for the commercial/industrial LULC class and ~ 30 $W m^{-2}$ and ~ 100 $W m^{-2}$ lower for the xeric and mesic residential LULC classes, respectively (Fig. 11a). Maximum H for the desert LULC are ~ 400 $W m^{-2}$, while they amount to ~ 430 , 370 and 300 $W m^{-2}$ for the three urban LULC classes. Even though z_0 is higher and albedo is lower for urban than for desert LULC, H from urban LULC are reduced due to urban landscape irrigation and relatively higher surface heat storage fluxes, G . Maximum G are reached at ~ 1100 LST with absolute values of ~ 400 W

m^{-2} , 290 W m^{-2} , 240 W m^{-2} for the three urban LULC classes. For the desert LULC, the maximum G is $\sim 150 \text{ W m}^{-2}$. Maximum λE of the desert and three urban (commercial/industrial, xeric, mesic) LULC classes are $\sim 90 \text{ W m}^{-2}$, $\sim 20 \text{ W m}^{-2}$, 140 W m^{-2} and $\sim 280 \text{ W m}^{-2}$, which amounts to λE differences of $\sim 70 \text{ W m}^{-2}$, 120 W m^{-2} and 190 W m^{-2} (Fig. 11b).

The largest differences in H between S_{urban} and S_{rural} ($\sim -280 \text{ W m}^{-2}$) occur in the irrigated agricultural areas to the west and southeast of the city. Those are accompanied by λE differences of $\sim 360 \text{ W m}^{-2}$ (Fig. 11b). The maximum λE values for the irrigated agricultural areas in S_{urban} are $\sim 440 \text{ W m}^{-2}$ and $\sim 80 \text{ W m}^{-2}$ for the desert LULC in S_{rural} . Consequently, the PBL heights are several hundred meters higher in S_{rural} than in S_{urban} (Fig. 11c) with the effects extended outside the city boundaries. Maximum PBL heights occur at about 1600 LST with magnitudes of 2700 m and 3600 m for S_{urban} and S_{rural} , respectively. Surface CAPE is also influenced by both H and λE . Irrigation and accompanying evapotranspiration rates cause CAPE to be higher by up to 500 J kg^{-1} in the irrigated agricultural areas (Fig. 11d) in S_{urban} (CAPE $\sim 1900 \text{ J kg}^{-1}$) as compared to S_{rural} (CAPE $\sim 1400 \text{ J kg}^{-1}$ for desert LULC in the same location). Within the city boundaries, landscaping irrigation did not compensate for the decrease in H and therefore CAPE is higher overall for desert LULC in S_{rural} ($\sim 1400 - 1500 \text{ J kg}^{-1}$) than for urban LULC ($\sim 1100 - 1400 \text{ J kg}^{-1}$).

These results highlight the fact that urban modifications of the surface energy balance of Phoenix, a city in a semi-arid environment, differ from those of cities in humid climates which are usually characterized by reduced λE and increased H in comparison to their rural environments. For the Phoenix metropolitan region, λE are higher and H is lower than in the rural area during daytime. In summary, the simulations for this particular event suggest that the Phoenix urban surface energy balance and PBL processes led to complex modifications in thunderstorm development in the region, affecting the upslope thermal flow, location and

wind speed of outflow from thunderstorms over the mountains, the convergence that supports new convection and location, and the amounts of precipitation.

c. Stein-Alpert Sensitivity study

1) EFFECTS OF URBAN SENSIBLE HEAT FLUXES

In order to quantify the effect of specific physical characteristics on the simulated P_{acc} , the Stein-Alpert technique (cp. paragraph 2c) was applied at 0500 LST 3 August 2005, after the storm has moved over the Phoenix region. Figure 12a shows the P_{acc} difference fields between S_{urban} and S_{rural} , ($f_{123} - f_0$). The contribution of the individual urban factors (1)-(3) and their interactions to ($f_{123} - f_0$), i.e. the fields Δf_1 , Δf_2 , Δf_3 , Δf_{12} , Δf_{13} , Δf_{23} and Δf_{123} (Table 2) are given in Figs. 12(b-h). Fig. 12c shows the differences in P_{acc} between S_2 and S_{rural} (Δf_2), which can be attributed to H_{urban} . In S_2 only urban H modifications were considered while the rural values of τ and λE were maintained.

Fig. 12c most closely resembles Fig. 12a, particularly near the urban fringe (except in the west) as well as within the southeastern part of the city. This suggests that H_{urban} contributed significantly to the differences between S_{urban} and S_{rural} . Urban H alone in S_2 would lead to a stronger reduction in P_{acc} in the center and higher P_{acc} to the northwest of the urban area in comparison with the combined effects of all urban factors and their interactions in S_{urban} . The Stein-Alpert technique was applied also to div_{surf} , 10 m wind speed, u_{10m} and direction, Ψ_{10m} . Fig. 13 (left panels) shows the div_{surf} difference fields ($f_{123}-f_0$) of S_{urban} and S_{rural} at 1500, 1600 and 1700 LST. For a clear visualization the difference fields ($f_{123}-f_0-\Delta f_2$) are given in Fig. 13 (right panels). Consequently, if the urban modifications in H contribute strongly to the simulated div_{surf} differences between S_{urban} and S_{rural} in a particular location the fields ($f_{123}-f_0-\Delta f_2$) should be small there. The 1500 LST plots were included in the analysis in order to detect if H_{urban} influenced the propagation of thunderstorms towards the city. The

analysis is carried out under the assumption that thunderstorms develop preferentially in areas of relatively high surface convergence, CAPE and PBL.

From Fig. 13 (right panels) at 1500 LST it can be concluded that the differences in the convergence area of the outflow of convection over the mountains and the westerly upslope flow between S_{urban} and S_{rural} (expressed in $(f_{123}-f_0)$ in Fig. 13, left panels) can be explained largely by H_{urban} , since the differences for $(f_{123}-f_0-\Delta f_2)$ in the convergence area disappear almost completely. Also H_{urban} contribute strongly to the differences in the location of convergence ($div_{surf} \sim -0.0001 \text{ s}^{-1}$) immediately south of the city, while differences related to the northwestwards propagation of storms from southeastern Arizona are influenced by H_{urban} to a much lesser extent (Fig. 13, right panels). The outflow from the storms over the mountains approaches the city with higher wind speeds ($\Delta u_{10m} \sim 5 \text{ ms}^{-1}$) in S_{rural} (not shown). According to the Stein-Alpert analysis for u_{10m} and Ψ_{10m} this is largely due to H_{urban} induced changes in div_{surf} and associated locations of convergence areas (results not shown). This is also the case for the flow to the south and the southeastern part of the urban area.

The sensible heat fluxes also have a significant effect in producing the div_{surf} differences at 1600 LST resulting from the initial urban convection in the McDowell Mountains (Fig. 13, right panels) and subsequent differences in P_{acc} (Fig. 12a and d.). However H_{urban} cannot explain results of $(f_{123}-f_0)$ for div_{surf} , that are located north of the city at $\sim 34^\circ\text{N}$ and $111^\circ 40'\text{W}$ as well as some of the div_{surf} differences south of the city. As discussed in sec. 3b, significant differences in Ψ_{10m} between S_{urban} and S_{rural} occur at 1600 LST within and near the city boundaries with winds being westerly for S_{urban} (Fig. 8a) and northwesterly for S_{rural} (Fig. 8b). The Stein-Alpert analysis indicates that those modifications in Ψ_{10m} are clearly the result of urban H modifications (not shown). At 1700 LST significant differences in P_{acc} near the northern fringe were detected between S_{urban} and S_{rural} ($f_{123}-f_0$), which can be

explained by H_{urban} (Fig. 13, left panels, 1700 LST) as can the differences in P_{acc} south of and within the city.

In summary, the Stein-Alpert analysis of the impact of the Phoenix specific urban LULC on P_{acc} , div_{surf} , u_{10m} and Ψ_{10m} suggests that the H_{urban} significantly affect the simulated urban vs. rural precipitation differences in the city and surrounding regions. However, H_{urban} did not contribute as much to a decrease in P_{acc} in the urban simulation in an extended area to the northwest of the city at $\sim 33^{\circ}20'N$ to $34^{\circ}20'N$; $112^{\circ}W$ to $113^{\circ}W$ and a P_{acc} increase that occurred to the west of the city at $\sim 33^{\circ}25'N$; $112^{\circ}40'W$ (Fig. 12c).

2) URBAN MOMENTUM FLUXES

In S_I , the roughness length for momentum was changed from the rural value of 0.1 to 0.8 m, 0.5 m and 0.5 m for the urban LULC (commercial/industrial, mesic and xeric respectively). All other characteristics of the natural land surface were unchanged. The P_{acc} differences between S_I and S_{rural} (Δf_1) can be attributed to τ_{urban} and are shown in Fig. 12b. Here, τ_{urban} do not significantly influence P_{acc} south of the city, but contribute significantly to a decrease in P_{acc} in an extended area to the northwest of the city (at $\sim 33^{\circ}20'N$ to $34^{\circ}20'N$; $112^{\circ}W$ to $113^{\circ}W$) and a P_{acc} increase west of the city (at $\sim 33^{\circ}25'N$; $112^{\circ}40'W$). Within the city boundaries τ_{urban} did not affect P_{acc} significantly in the eastern part, but reduced P_{acc} in the central urban area in comparison with the fully urbanized model version (Fig. 12b). Urban momentum fluxes contributed to the P_{acc} reductions at the northeastern and southern fringe that were detected in Fig. 12a, however to a lesser degree than H_{urban} .

The results ($f_{123}-f_0$) for div_{surf} (Fig. 14, left panels), u_{10m} and Ψ_{10m} and the Stein-Alpert difference fields ($f_{123}-f_0-\Delta f_1$) were analyzed for 1500, 1600 and 1700 LST. According to Fig. 14b, τ_{urban} do not significantly affect the flow surrounding the city at 1500 LST and cannot explain the differences in div_{surf} , u_{10m} and Ψ_{10m} north and south of the city. However,

differences in u_{10m} within the city boundaries can be attributed to urban roughness effects (not shown). High τ_{urban} are accompanied by a reduction in mean horizontal wind speed due to an increased vertical momentum transfer in S_{urban} vs. S_{rural} . Also at 1600 LST τ_{urban} have no major effect on div_{surf} (Fig. 14, right panels), u_{10m} and Ψ_{10m} differences. However, τ_{urban} can explain some results of $(f_{123}-f_0)$ for div_{surf} , that are located north of the city at $\sim 34^\circ\text{N}$ and $111^\circ40'\text{W}$ and also within the city at 1700 LST (Fig. 14, right panels). In summary, the Stein-Alpert analysis shows that τ_{urban} did not significantly affect the onset of the convection on the northern fringe of the urban area, to the east and west of the McDowell Mountains and the convection within the city, but it impacted the storm movement towards the northwest and also modified the precipitation on the southern fringe.

3) EFFECTS OF URBAN LATENT HEAT FLUXES

The difference in P_{acc} between S_3 and S_{rural} (Δf_3) is shown in Fig. 12d. Urban effects on λE are considered in the S_3 simulations by incorporating irrigation for the urban and agricultural LULC classes (cp. paragraph 2c). All other characteristics were unchanged. Overall λE_{urban} contribute less to changes in precipitation than H_{urban} and τ_{urban} , but it adds to the differences in P_{acc} between S_{urban} and S_{rural} (Fig. 12a) in the eastern part of the urban area as well as the fringe regions, with the sign of the differences depending on the location. Higher P_{acc} west of the city at $\sim 33^\circ20'\text{N}$, $112^\circ40'\text{W}$ and lower P_{acc} values at $\sim 33^\circ45'\text{N}$, $112^\circ40'\text{W}$ for S_{urban} , can be attributed partly to urban modifications in λE (Fig. 12d). Those areas are near extensive irrigated agricultural fields that are characterized by relatively higher CAPE values in S_{urban} in comparison to S_{rural} (Fig. 11d). This result is in agreement with the Stein-Alpert analysis of λE_{urban} effects on div_{surf} , u_{10m} and Ψ_{10m} , which demonstrate that λE does not significantly affect the air flow in and surrounding the city prior to and during the occurrence of thunderstorms in the urban area (not shown). The analysis suggests that an

increase in atmospheric water vapor content through agricultural and landscaping irrigation is not a major factor influencing this particular convective event. However, irrigation and subsequent evapotranspiration rates affected precipitation significantly by modifying H_{urban} . Also evapotranspiration from irrigated landscapes may have increased the atmospheric moisture content in the region for a longer time period before the storm development.

4) NON-LINEAR INTERACTIONS OF URBAN PHYSICAL FACTORS

Figures 12 (e-h) show that the synergistic, non-linear interactions of τ_{urban} , H_{urban} and λE_{urban} influence P_{acc} strongly. Scenario S_{12} captures the interaction of τ_{urban} and H_{urban} and the contribution to S_{urban} , Δf_{12} (cp. Tab. 2), is shown in Fig. 12e. The most pronounced effects are an increase in P_{acc} in the central urban area and a reduction in P_{acc} west and northwest of the city. The interaction of τ_{urban} and H_{urban} captures the positive feedback between the two factors. An increase in τ_{urban} in WRF leads to an increase in the surface diffusion coefficients for heat and momentum and therefore an enhanced transport of thermal energy into the PBL. Hence, the interaction of τ_{urban} and H_{urban} acts to warm the PBL and increase CAPE over the city.

The influence of synergistic effects of τ_{urban} and λE_{urban} (simulated in S_{13}) on P_{acc} in S_{urban} is expressed in Δf_{13} (Fig. 12f). The effect is also relatively strong and leads to a significant increase in P_{acc} northwest of the city and in the urban area. An increase in τ in WRF leads to an increase in the surface diffusion coefficients for moisture and momentum and therefore an enhanced transport of moisture into the PBL. Figure 12g shows the effects of the interaction of λE_{urban} and H_{urban} (simulated in S_{23}) on P_{acc} as captured by Δf_{23} . As for the other two-factor interactions an increase in P_{acc} in the center of the urban area was detected. The λE_{urban} lead to an increase in CAPE because of higher levels of atmospheric moisture. The interaction of all three urban factors, τ_{urban} , H_{urban} and λE_{urban} (simulated in S_{urban}) as

represented by Δf_{123} in Fig. 12h has the strongest effect on P_{acc} and appears to enhance features that are also captured by the response of P_{acc} to the individual factors, especially Δf_1 and Δf_2 (Fig. 12b-c).

It can be concluded that the synergistic terms have a strong effect on P_{acc} , especially in the central part and west/northwest of the city. However, the superposition of the interaction terms in S_{urban} cancels the strong impact on P_{acc} in the eastern part of the city and the northern and eastern fringe regions such that H_{urban} are the dominant effect there. The superposition of all single-factor and synergistic terms leads to the simulated differences in P_{acc} between S_{urban} and S_{rural} in the central urban area.

4. Conclusions

In this study WRF was used to investigate urban effects on a convective event on 02-03 August 2005 in the Phoenix Metropolitan region. The results show that urban physical characteristics significantly affected the amount and location of precipitation in and surrounding the urban area. In agreement with observations, accumulated precipitation was lower within the urban area and higher at the northern fringe of the city in a simulation with urban LULC and physical characteristics included, in comparison to a simulation with the native desert LULC. A Stein-Alpert sensitivity analysis was carried out in order to investigate the contribution of λE_{urban} , τ_{urban} , and H_{urban} and their interactions on the differences in precipitation between the two LULC scenarios.

In agreement with studies for urban areas in more humid environments, it is suggested that urban H modifications have the most pronounced effect on P_{acc} within and near the urban boundary while the effects of increased τ_{urban} and λE_{urban} were relatively weaker. Particularly, the increase in precipitation on the northern fringe of the urban area are due to H_{urban} , as is the precipitation reduction in the eastern part of the city. The multi-factor non-linear interaction

terms have a strong effect on the P_{acc} in the central urban area and west of the city. However, superposition of the interaction terms in S_{urban} in part cancels the strong impact on P_{acc} . But, in comparison with cities in more humid environments, urbanization has the opposite effect on sensible heat fluxes in this arid region, i.e. due to landscaping irrigation and high heat storage fluxes, H_{urban} is lower than in the rural surroundings. Maximum urban PBL heights in Phoenix are several hundred meters lower than for rural LULC with the effects extended outside the city boundaries. Reduced H_{urban} caused overall divergence in the urban area. The divergence flow collides with the westerly flow at the northern fringe of the city and thus enhances precipitation there. Consequently, the main mechanisms by which H_{urban} modify convection in the semi-arid and mountainous Phoenix region are fundamentally different from those in more humid environments. For the latter an urban increase in sensible heat fluxes causes drier and higher PBL's and low-level convergence that is favorable for generating cumulonimbus clouds and initiating convection downwind of the city (Cotton and Pielke 2007). Also in the Phoenix metropolitan area agricultural and landscaping irrigation lead to enhanced CAPE values in some parts of the urban region. In contrast, Rozoff et al. (2003) reported a decrease in CAPE for St. Louis despite the increase in H for urban LULC in comparison with the natural surroundings due to reduced evapotranspiration rates. The model results indicate also a more complex response to urban H modifications for Phoenix. According to WRF, the reduction in H_{urban} modifies the storm propagation from the mountains into the Phoenix metropolitan region by affecting the interaction of thunderstorm outflow with the thermal upslope flow, thereby changing locations of convergence zones.

Our study supports findings by Diem and Brown (2003) and Shepherd et al. (2006) who showed a large historic increase in precipitation for weather stations located in the Verde Valley River Basin northwest of Phoenix. For that particular area, our simulation showed an enhanced precipitation in S_{urban} as well. However, our results do not support their hypothesis

that the enhanced precipitation is due to irrigation and a subsequent increase in atmospheric moisture in the Verde Valley region. According to this study the increased precipitation is clearly due to urban modifications in sensible heat fluxes. However, evapotranspiration from irrigated landscapes may have increased the atmospheric moisture content in the region for a longer time period prior to the storm development. Also, irrigation has an indirect effect on precipitation by significantly modifying surface sensible heat fluxes.

Because this is the first detailed modeling analysis of a convective event in this urban area, caution is advised before general conclusions can be drawn on the influence of urbanization on convection in Phoenix. However, the study of this particular convective event provides a template for subsequent model experiments to be performed using a similar methodology. Currently, other case studies are analyzed in order to draw generalizable results.

Acknowledgements

This material is based upon work supported by the National Science Foundation under Grants ATM-0710631, ATM-813656 and DEB-0423704, Central Arizona - Phoenix Long-Term Ecological Research (CAP LTER). Any opinions, findings and conclusions or recommendation expressed in this material are those of the authors and do not necessarily reflect the views of the National Science Foundation. The research is also funded by Science Foundation Arizona (grant CAA 0228-08) and NCAR's Advanced Study Program. Mr. Stephen Bieda III provided technical assistance with WRF model simulations and meteorological analyses during the early stages of this project.

References

- Adams, D.K., and A.C. Comrie, 1997, The North American Monsoon, *Bull. Amer. Meteor. Soc.*, **78**, 2197-2213.
- Anderson, J. R., Hardy, E. E., Roach, J. T., and R. E. Witmer, 1976: *A Land Use and Land Cover Classification System for Use with Remote Sensor Data*. Geological Survey Professional Paper 964, U.S. Government Printing Office, 28 pp.
- Balling, R.C. Jr., and S.W. Brazel, 1987a: Diurnal Variations in Arizona Monsoon precipitation frequencies, *Monthly Weather Review*, **115**, 342-346.
- Balling, R.C. Jr., and S.W. Brazel, 1987b: Recent changes in Phoenix, Arizona summertime diurnal precipitation patterns, *Theor. Appl. Climatol.*, **38**, pp. 50-54.
- Bornstein, R., and M. LeRoy, 1990, Urban barrier effects on convective and frontal thunderstorms, Fourth AMS Conference on mesoscale Processes, Boulder, CO, 25-29 June.
- Bornstein, R., and Q. Lin, 2000, urban heat island and summertime convective thunderstorms in Atlanta: three case studies, *Atmospheric Environment*, **34**, 507-516.
- Bright, D.R., and S.L. Mullen, 2002, The sensitivity of the numerical simulation of the southwest monsoon boundary layer to the choice of PBL turbulence parameterizations in MM5, *Weather and Forecasting*, **17**, 99-114.
- Bryson, R and W.P. Lowry, 1955: Synoptic climatology of the Arizona summer precipitation singularity. *Bull.Amer.Meteor.Soc.*, **36**, 329-339.
- Burian, S.J., and J.M. Shepherd, 2005, Effect of urbanization on the diurnal rainfall pattern in Houston, *Hydrological Processes*, **19**, 1089-1103.
- Changnon, S.A., Jr., 1981, *METROMEX: A review and summary*. Changnon, S.A., Jr., (ed.), pp. 181, American Meteorological Society, Meteorological Monographs, **18**, No.40.
- Changnon, S.A., 2001, Assessment of historical thunderstorm data for urban effects: the Chicago case, *Climatic Change*, **49**, 161-169.

- Chen, F., Janjic, Z., and K. Mitchell, 1997: Impact of the atmospheric surface-layer parameterizations in the new land-surface scheme of the NCEP mesoscale Eta model. *Boundary-Layer Meteor.*, **85**, 391-421.
- Chen, S.-H., and W.-Y. Sun, 2002, A one-dimensional time dependent cloud model. *J. Meteor. Soc. Japan*, **80**, 99–118.
- Collins, W. D., Rasch, P. J., Boville, B. A., Hack, J. J., McCaa, J. R., Williamson, D. L., Kiehl, J. T., and B. Briegleb, 2004: Description of the NCAR Community Atmosphere Model (CAM 3.0). NCAR Technical Note 464+STR, pp 102-106.
- Cotton, W.R., and R.A. Pielke, 2007, *Human impacts on climate*, pp. 330, Cambridge University Press.
- Diem J.E., and D.P. Brown, 2003, Anthropogenic impacts on summer precipitation in central Arizona, U.S.A., *The Professional Geographer*, **55**, 343-355.
- Janjic, Z. I., 2002: *Nonsingular Implementation of the Mellor–Yamada Level 2.5 Scheme in the NCEP Meso model*. NCEP Office Note, No. 437, 61 pp.
- Grossman-Clarke, S., Zehnder, J. A., Loridan, T., and C. S. B. Grimmond, 2010: Contribution of Land Use Changes to Near Surface Air Temperatures during recent Summer Extreme Heat Events in the Phoenix Metropolitan Area. *J. Appl. Meteorol. and Climatol.*, 49 (8), pp. 1649-1664.
- Grossman-Clarke, S., Zehnder, J. A., Stefanov, W. L., Liu, Y., and M. A. Zoldak, 2005: Urban Modifications in a Mesoscale Meteorological Model and the Effects on Surface Energetics in an Arid Metropolitan Region. *J. Appl. Meteorol.*, **44**, 1281–1297.
- Hales Jr., J. E., 1977. On the relationship of convective cooling to nocturnal thunderstorms in Phoenix. *Monthly Weather Review*, 105, 1609-1613.
- Hales, J.E., 1972: Surges of maritime tropical air northward over the Gulf of California. *Mon.Wea.Rev.*, **100**, 298-306

- Hand, L. and J. M. Shepherd, 2009: An investigation of warm season spatial rainfall variability in Oklahoma City: Possible linkages to urbanization and prevailing wind. *Journal of Applied Meteorology and Climatology*, **48**: 251–269.
- Heinselman, P. L. and D. M. Schultz 2006: Intraseasonal Variability of Summer Storms over Central Arizona during 1997 and 1999. *Weather and Forecasting*, **21**, 559-578.
- Holton, J. R., 1967: The diurnal boundary layer wind oscillation above sloping terrain. *Tellus* XIX, 200-205.
- Kain, J. S., 2004: The Kain–Fritsch Convective Parameterization: An Update. *Journal of Applied Meteorology*, **43**, 170–181.
- Kusaka, H., and F. Kimura, 2004: Thermal Effects of Urban Canyon Structure on the Nocturnal Heat Island: Numerical Experiment Using a Mesoscale Model Coupled with an Urban Canopy Model. *Journal of Applied Meteorology*, **43**, 1899-1910.
- Lin, Y.-L., Farley, R. D., and Orville, H. D. 1983: Bulk parameterization of the snow field in a cloud model, *J. Appl. Meteor.*, 22, 1065–1092.
- Maddox, R. A., D. M. McCollum, and K. W. Howard, 1995, Large-scale patterns associated with severe summertime thunderstorms over central Arizona. *Wea. Forecasting*, **10**, 763-778.
- Orville, R.E., Huffines, G., Nielsen-Gammon, J., Zhang, R., Ely, B., Steiger, S. Phillips, S., Allen, S., and W. Read, 2001, Enhancement of Cloud-to-Ground Lightning over Houston, Texas, *Geophysical Research Letters*, **28**, 2597-2600.
- Rozoff, C.M., Cotton, W.R., and J.O. Adegoke, 2003, Simulation of St. Louis, Missouri, land use impacts on thunderstorms, *J. Appl. Meteorol.*, 42, 716-738.
- Shem, W. and J. M. Shepherd 2009: On the impact of urbanization on summertime thunderstorms in Atlanta: Two numerical model case studies. *Atmospheric Research*, **92**, 172-189.

- Shepherd, J. M., Carter, M., Manyin, M., Messen, D., and S. Burian, 2010: The impact of urbanization on current and future coastal precipitation: a case study for Houston. *Environment and Planning B: Planning and Design*, **37**, 284-304.
- Shepherd, J.M., 2006: Evidence of urban-induced precipitation variability in arid climate regimes *Journal of Arid Environments*, **67**, 607–628.
- Shepherd, J.M., 2005: A review of current investigations of urban-induced rainfall and recommendations for the future, *Earth Interactions*, **9**, 1-27.
- Skamarock, W. C., Klemp, J. B. , Dudhia, J., Gill, D. O., Barker, D. M., Wang W., and J. G. Powers, 2005: A Description of the Advanced Research WRF Version 2. NCAR Technical Note-468+STR, 88 pp.
- Smith, W.P., and R. L Gall, 1989: Tropical squall lines of the Arizona monsoon. *Monthly Weather Review*, **117**, 1553-1569.
- Stein, U. and P. Alpert, 1993: Factor separation in numerical simulations. *J. of the Atmospheric Sciences*, **50**, 2107-2115.
- Svoma, B. M., 2010: The influence of monsoonal gulf surges on precipitation and diurnal precipitation patterns in central Arizona. *Weather and Forecasting*, **25**, 281-289.

Table 1: Scenarios carried out to separate the influence of urban momentum, sensible and latent heat flux according to Stein and Alpert (1993).

Urban modifications→ Scenario↓	Momentum flux	Sensible heat flux	Latent heat flux	Simulated fields
S_{rural}	τ_{rural}	H_{rural}	λE_{rural}	f_0
S_1	τ_{urban}	H_{rural}	λE_{rural}	f_1
S_2	τ_{rural}	H_{urban}	λE_{rural}	f_2
S_3	τ_{rural}	H_{rural}	λE_{urban}	f_3
S_{12}	τ_{urban}	H_{urban}	λE_{rural}	f_{12}
S_{13}	τ_{urban}	H_{rural}	λE_{urban}	f_{13}
S_{23}	τ_{rural}	H_{urban}	λE_{urban}	f_{23}
S_{urban}	τ_{urban}	H_{urban}	λE_{urban}	f_{123}

Table 2: Difference fields Δf_i that express the contribution of the factors (1) to (3) and their interactions to the simulated difference fields obtained from S_{urban} minus S_{rural} (Table 1).

Symbol	Difference
Δf_0	f_0
Δf_1	$f_1 - f_0$
Δf_2	$f_2 - f_0$
Δf_3	$f_3 - f_0$
Δf_{12}	$f_{12} - (f_1 + f_2) + f_0$
Δf_{13}	$f_{13} - (f_1 + f_3) + f_0$
Δf_{23}	$f_{23} - (f_2 + f_3) + f_0$
Δf_{123}	$f_{123} - (f_{12} + f_{13} + f_{23}) + (f_1 + f_2 + f_3) - f_0$

Figure 1: (a) USGS Land Use/Land Cover (LULC) data for the Phoenix metropolitan region. Shown are: \circ irrigated agriculture; ∇ deciduous broadleaf vegetation (riparian vegetation) and three urban LULC categories: \bullet urban-built-up; $+$ mesic residential; and \blacktriangleright xeric residential. The USGS “shrubland” LULC class is assigned to the areas surrounding the city and represents the native desert vegetation (for simplification no symbols are included); (b) Contours of terrain (elevation intervals of 300m); city boundaries (gray outline) and National Weather Service station at Sky Harbor Airport (black dot).

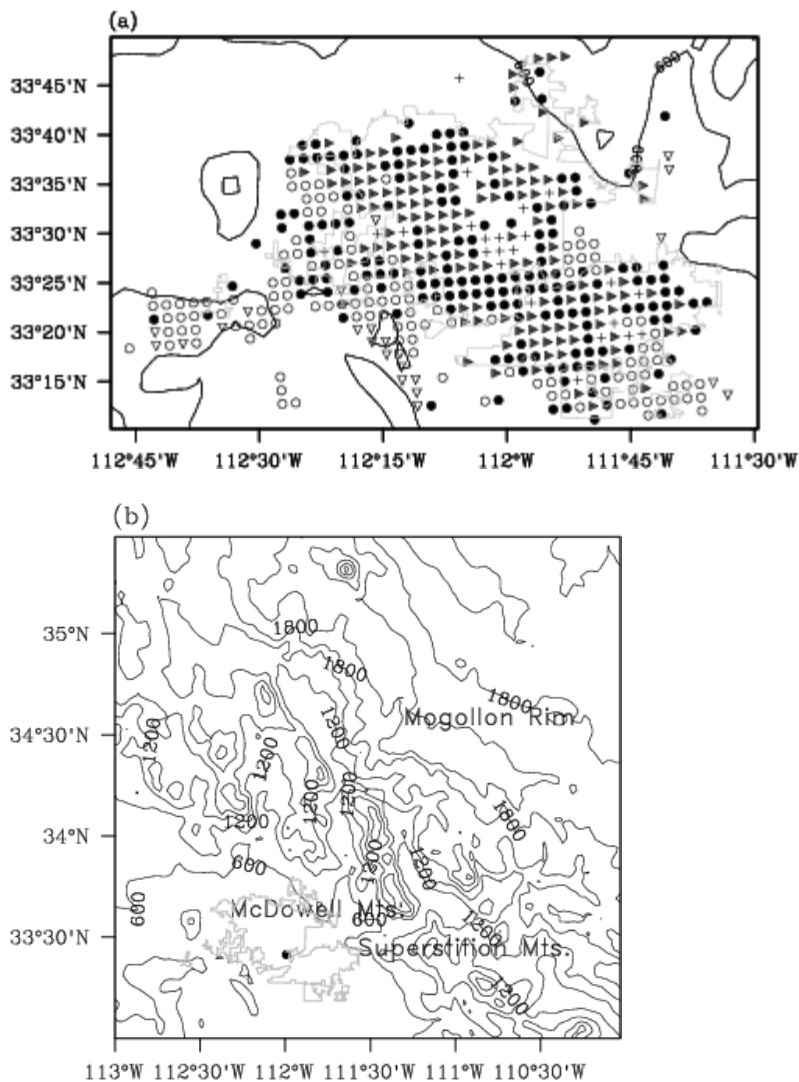


Figure 2: Contours of 500 hPa (a) geopotential heights (contours from 5760 m to 5940 m in intervals of 30 m) and (b) mixing ratio (contours from 0 gkg^{-1} to 5 gkg^{-1} in intervals of 0.5 gkg^{-1}) at 00 UTC 3 August 2005.

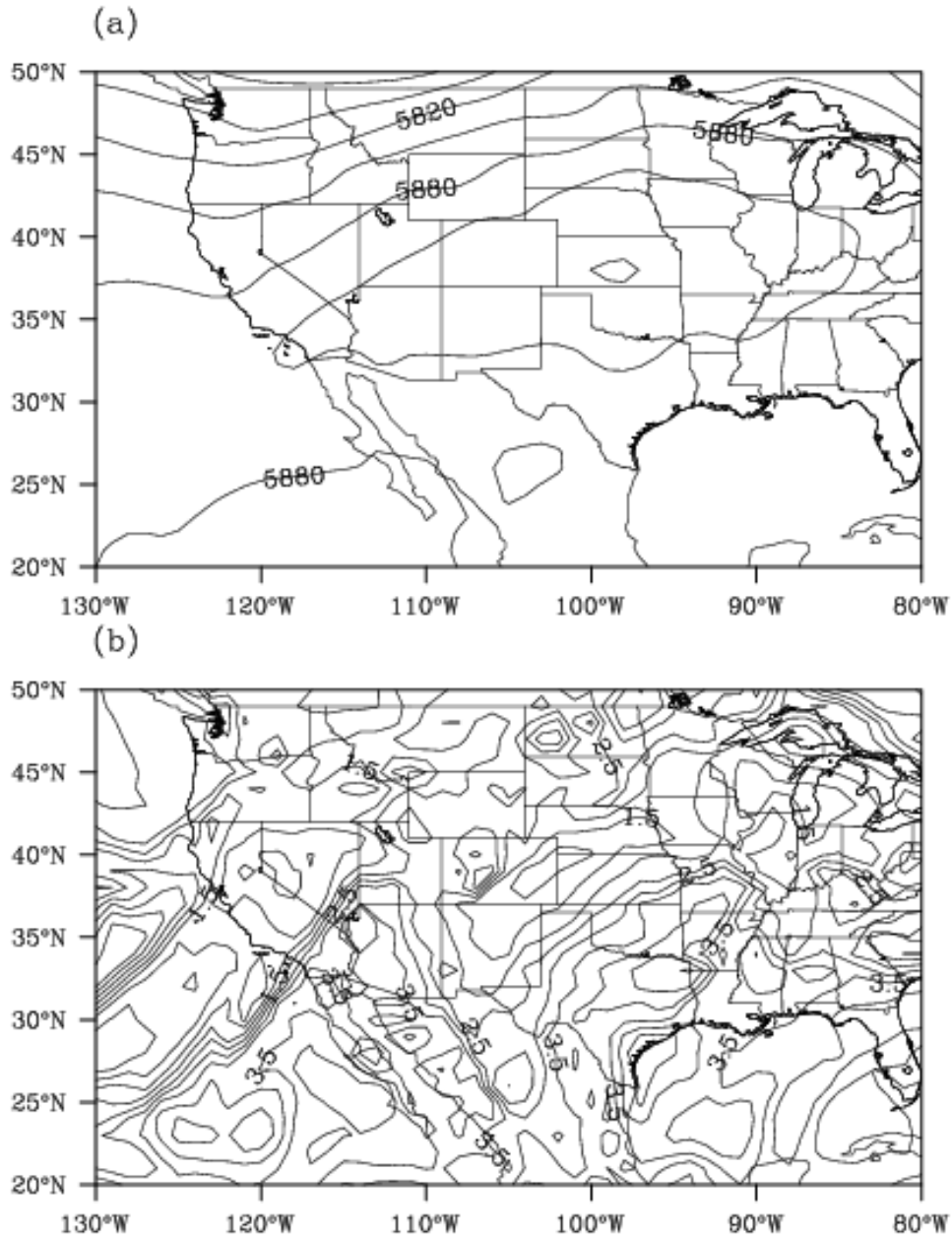


Figure 3: Measured profiles of air temperature in °C (black), dew point temperature in °C (gray), and wind speed and direction at Sky Harbor Airport at (a) 0000 UTC 3 August 2005 (1700 LST 2 August 2005) and (b) 1200 UTC 3 August 2005 (0500 LST 3 August 2005).

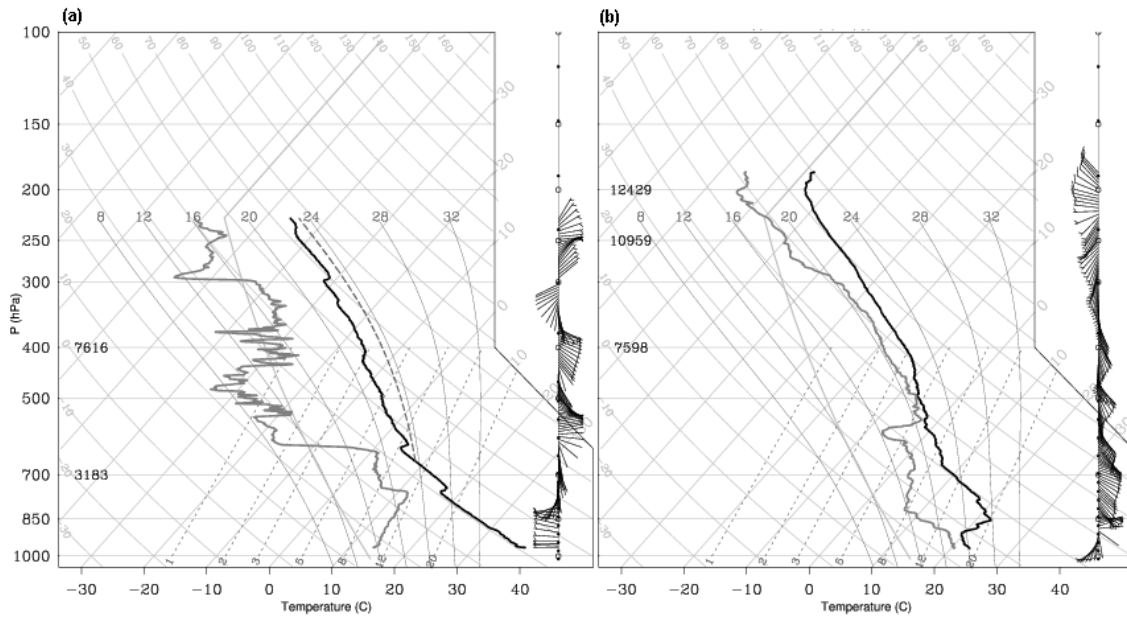


Figure 4: Accumulated hourly precipitation (mm) for (a) 1100 LST to 1700 LST, 02 August 2005 and (b) 1800 LST, 02 August 2005 to 0000 LST, 03 August 2005 for NCEP Stage IV analysis (left column) and WRF simulated (right column).

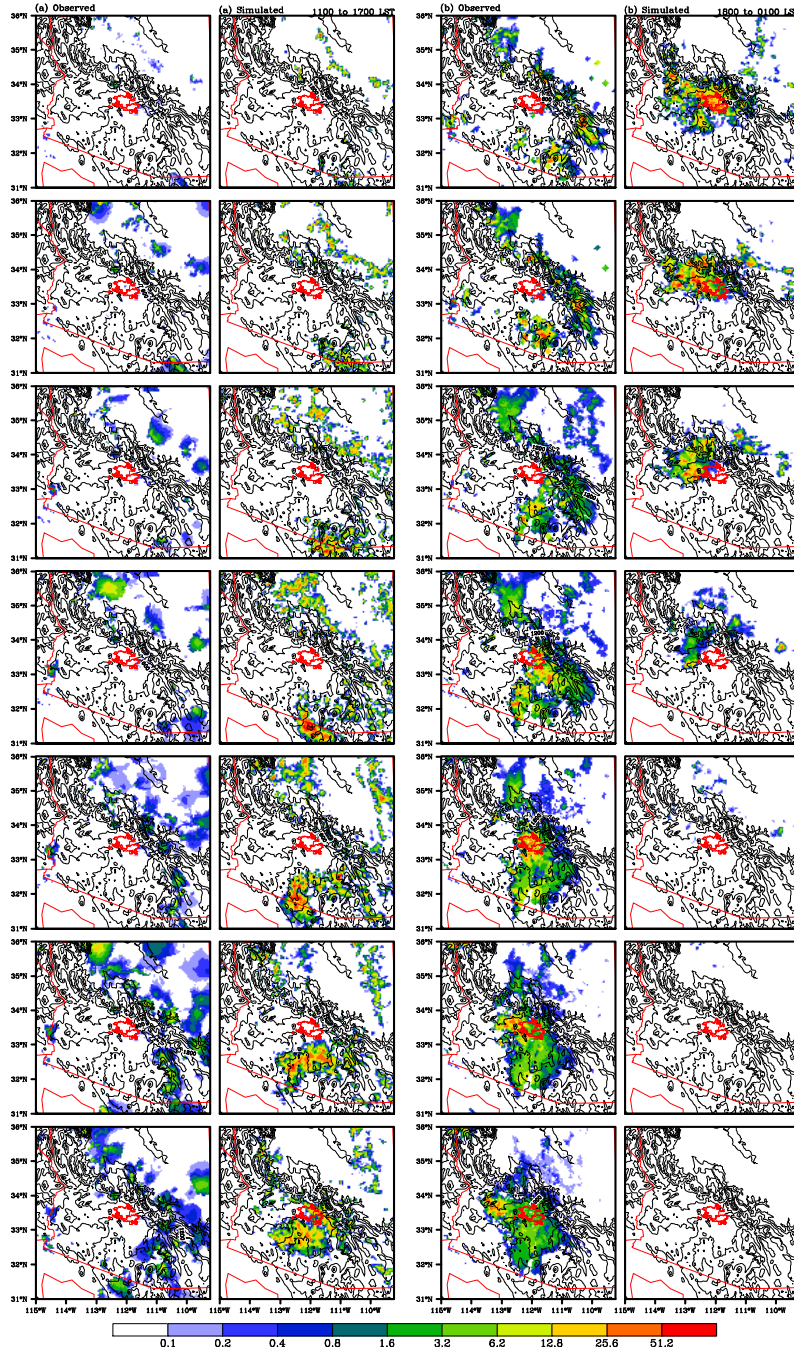


Figure 5: Three WRF modeling domains with resolutions of 30, 10 and 2.5 km, respectively.

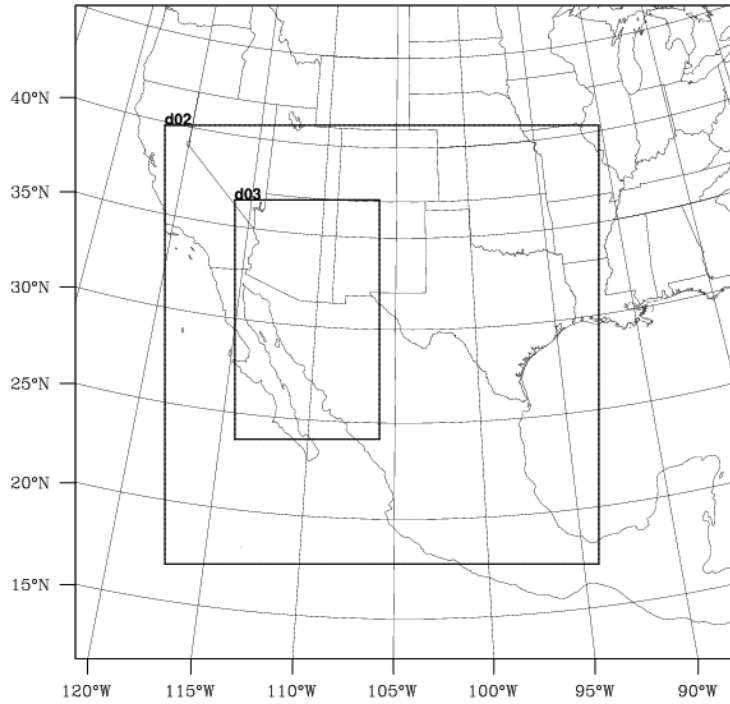


Figure 6: Observed and simulated soundings at Phoenix Sky Harbor Airport for (a) 18 UTC 2 August 2005 and (b) 00 UTC 3 August 2005 (gray dashed line – observed dew point temperature; gray solid line – observed air temperature; black dashed line – simulated dew point temperature; black solid line – simulated air temperature).

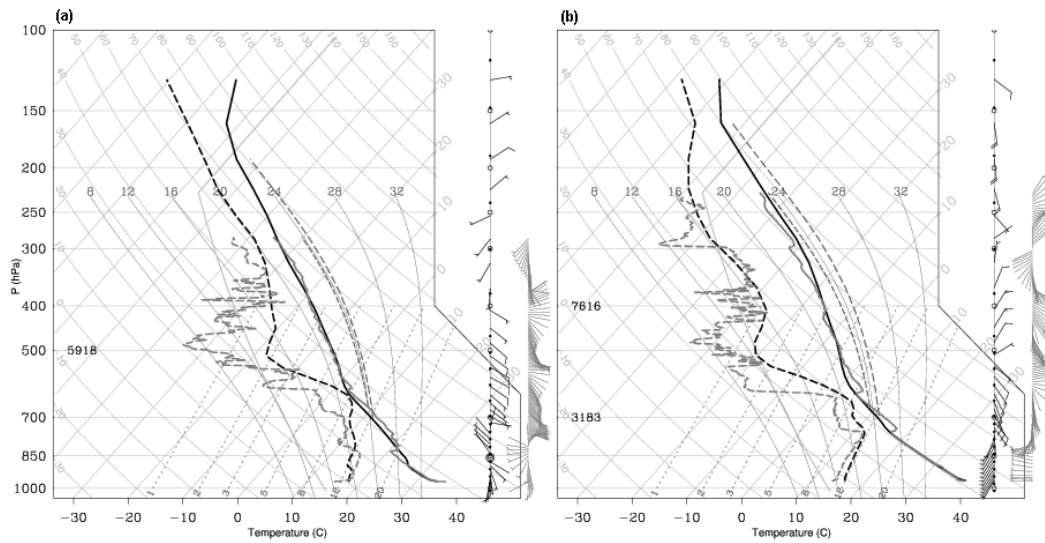


Figure 7: Surface divergence (s^{-1}) and surface wind fields at 1300, 1500 and 1600 LST, 02 August 2005 for (a) S_{urban} and (b) S_{rural} . City boundaries are outlined in red and black contour lines for terrain (elevation interval 300m).

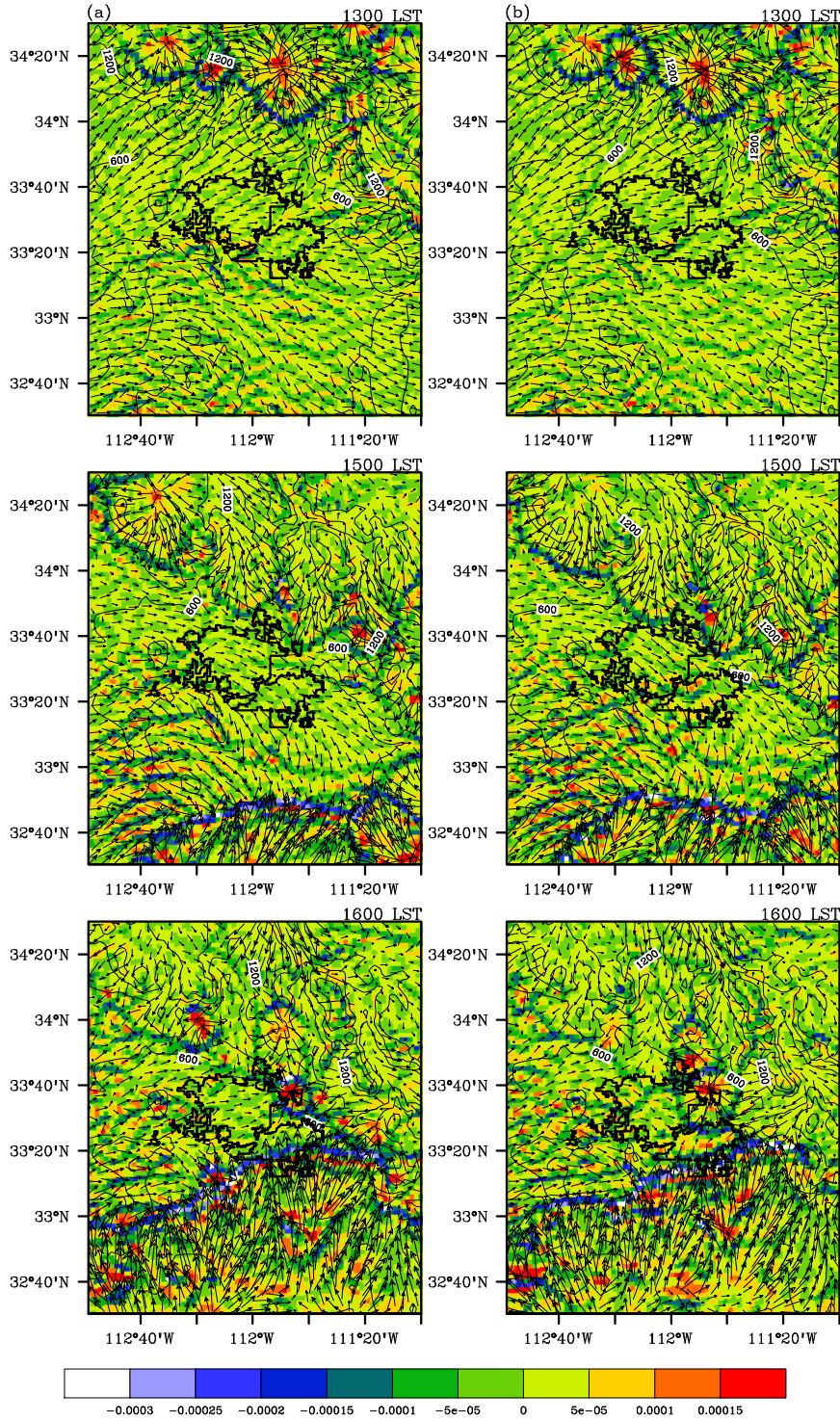


Figure 8: Surface divergence (s^{-1}) for the scenarios S_{urban} (left panel) and S_{rural} (right panel) at (a) 1500 LST, (b) 1600 LST and (c) 1650 LST 02 August 2005. City boundaries are outlined in black.

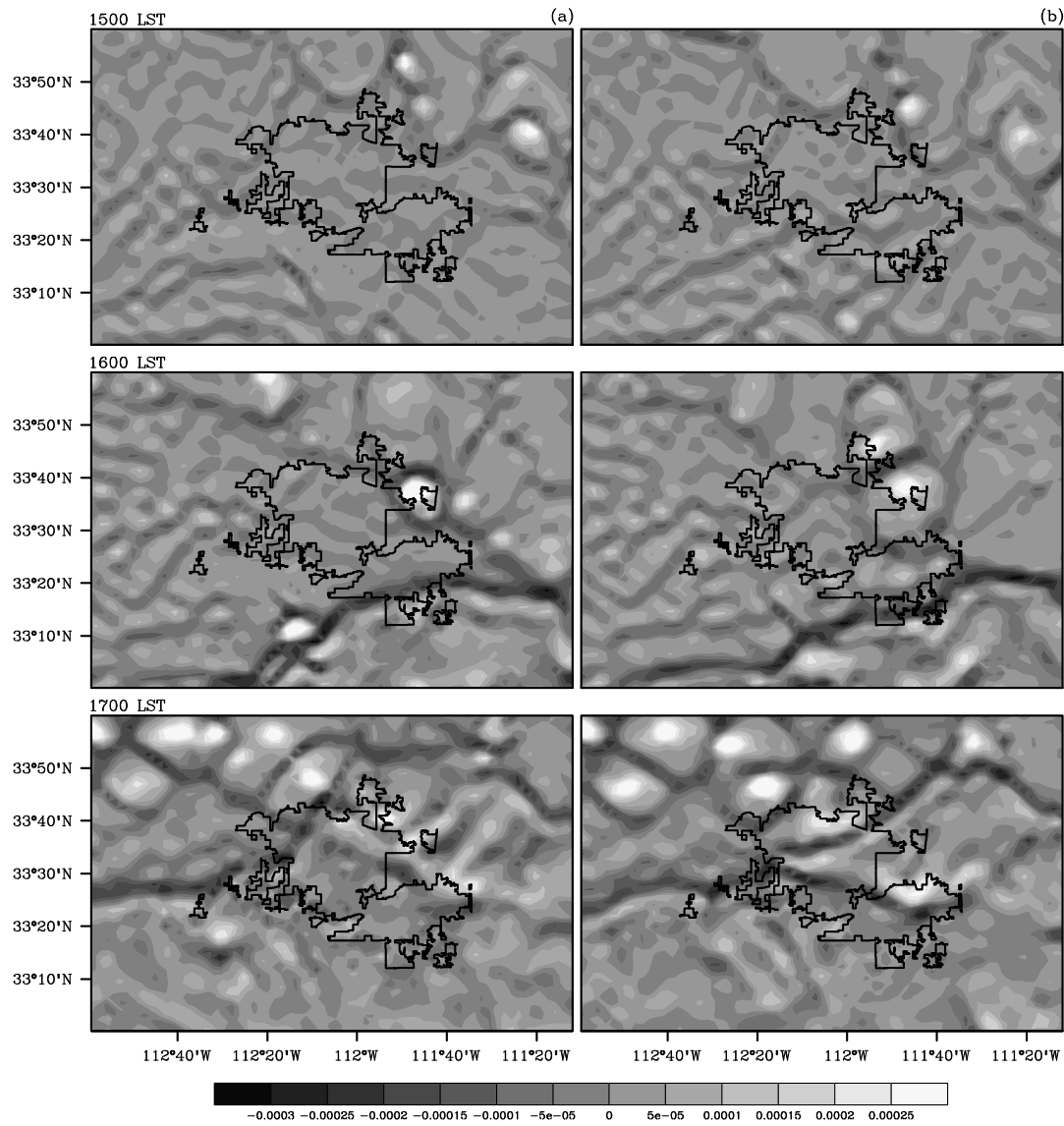


Figure 9: Accumulated precipitation (mm) within 30 minutes prior to 1600, 1630, 1700, 1730, 1800 and 1830 LST, 2 August 2005 for the scenarios (a) S_{urban} and (b) S_{rural} . City boundaries are outlined in red and black contour lines for terrain (elevation interval 300m).

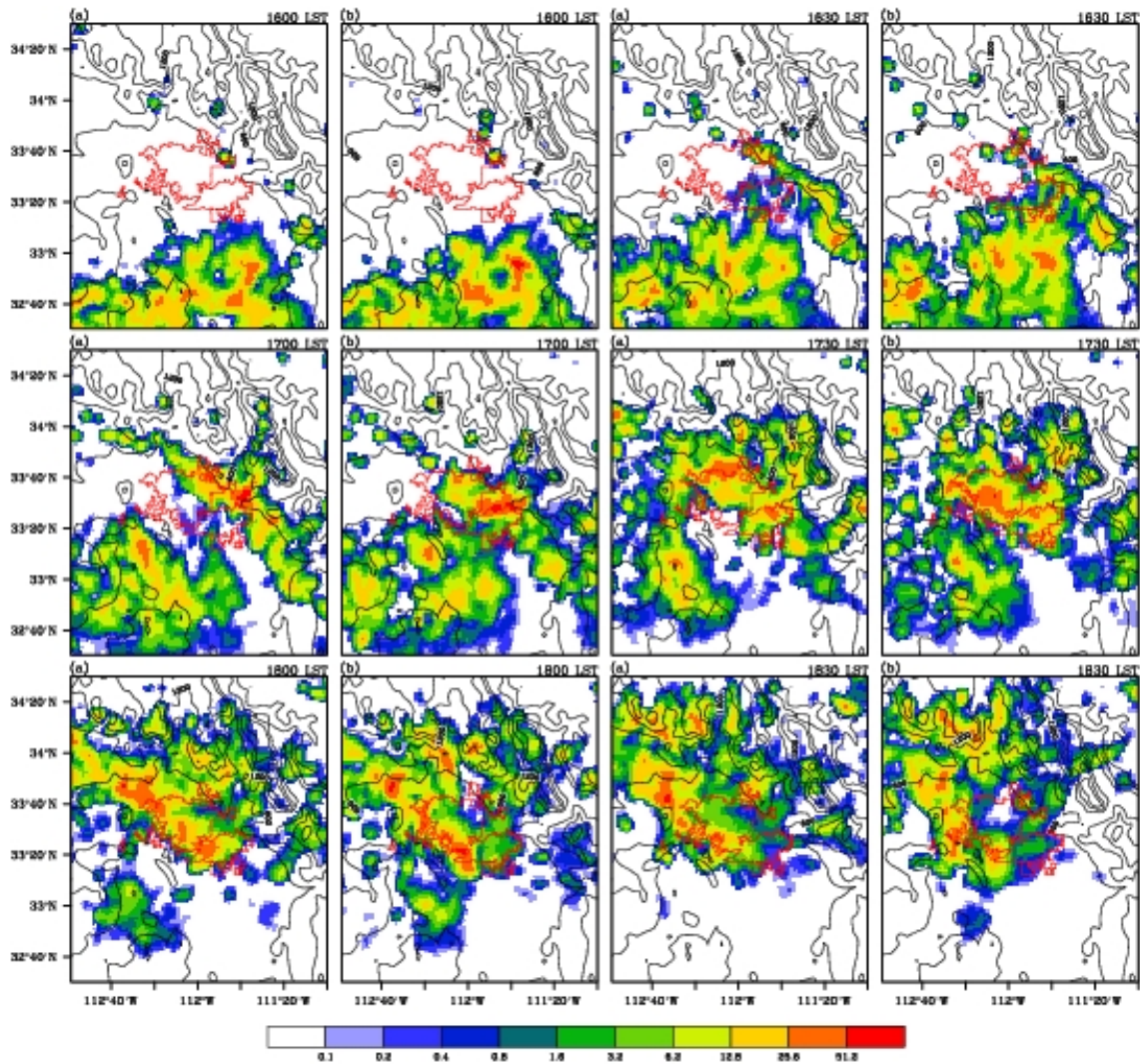


Figure 10: 24-hour accumulative precipitation (mm) at 0500 LST, 03 August 2005 of NCEP Stage IV precipitation analysis and the simulations for the scenarios S_{urban} and S_{rural} , as well as the differences between the two runs (S_{urban} minus S_{rural}). City boundaries are outlined in red and black contour lines for terrain (elevation interval 300 m).

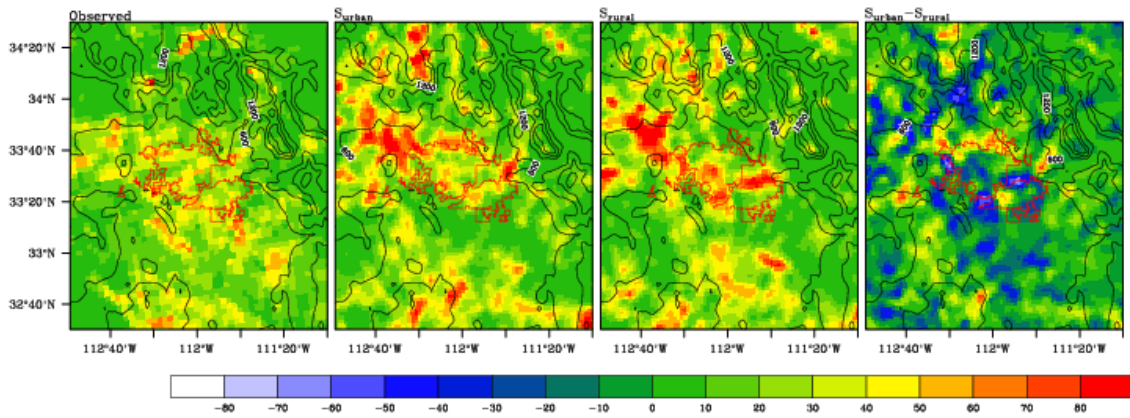


Figure 11: Simulated differences (S_{urban} minus S_{rural}) in sensible and latent heat fluxes, H and λE , respectively, boundary layer heights, PBL, and CAPE in the Phoenix region before the thunderstorm event at 1300 LST, 2 August 2005. City boundaries are outlined in black.

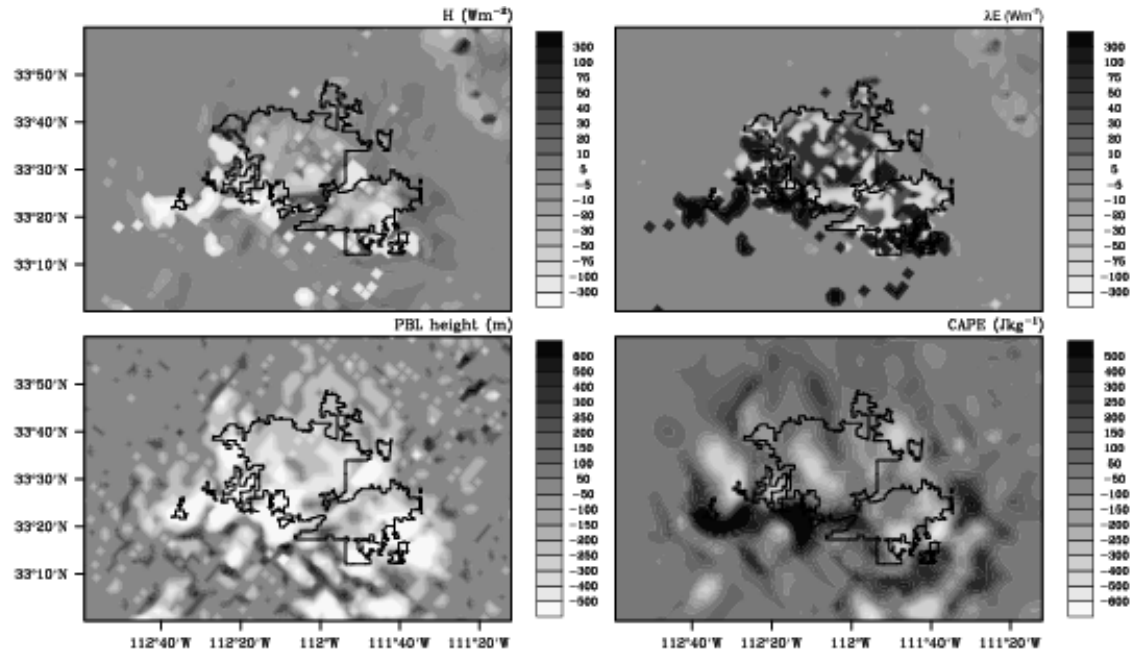


Figure 12: Results from the Stein-Alpert sensitivity analysis for accumulated precipitation (mm) at 0500 LST 3 August 2005 with (a) $f_{123}-f_0$; (b) f_1-f_0 ; (c) f_2-f_0 ; (d) f_3-f_0 ; (e) $f_{12} - (f_1 + f_2) + f_0$; (f) $f_{13} - (f_1 + f_3) + f_0$; (g) $f_{23} - (f_2 + f_3) + f_0$ and (h) $f_{123} - (f_{12} + f_{13} + f_{23}) + (f_1 + f_2 + f_3) - f_0$ (cp. Tables 1 and 2). The outline of the urban area is included in black.

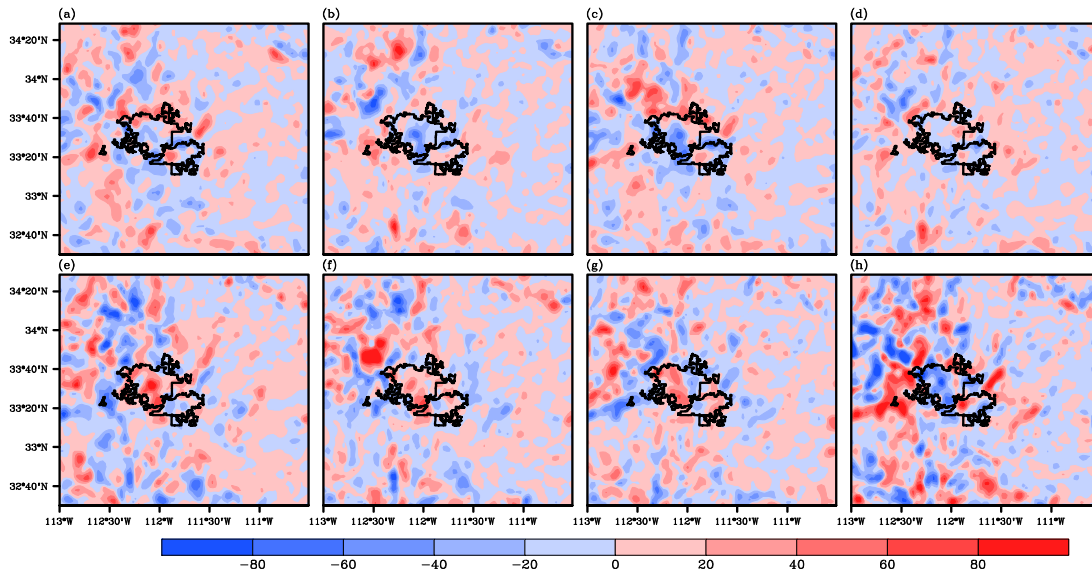


Figure 13: Results from the Stein-Alpert sensitivity analysis to investigate effects of urban H on surface divergence, $div_{surf}(s^{-1})$ at 1500, 1600 and 1700 LST 2 August 2005 with difference fields $(f_{123}-f_0)$ in the left panels and $(f_{123}-f_0-\Delta f_2)$ in the right panel. The outline of the urban area is included in black.

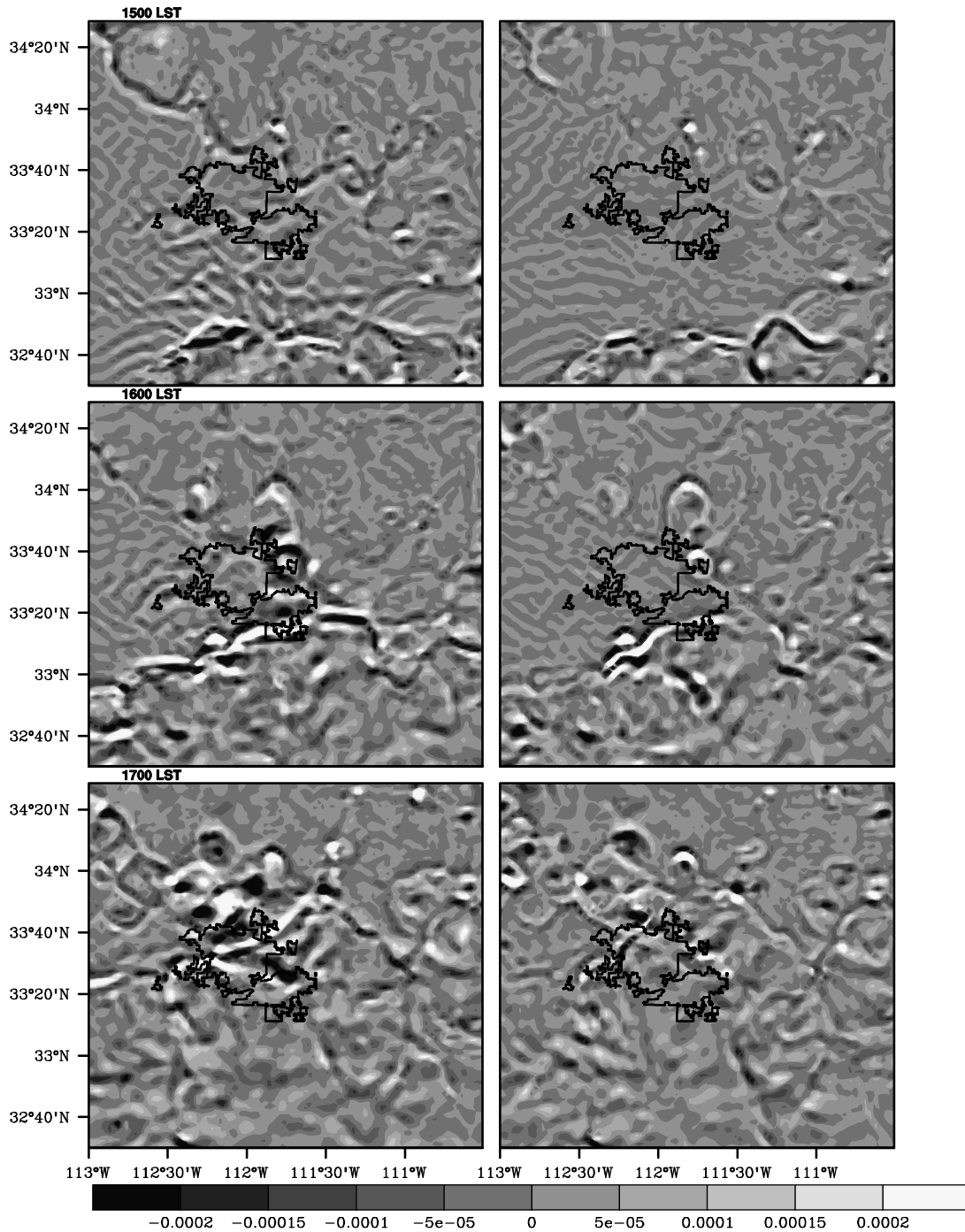


Figure 14: Results from the Stein-Alpert sensitivity analysis to investigate effects of $z_{0,urban}$ on surface divergence, $div_{surf}(s^{-1})$ at 1500, 1600 and 1700 LST 2 August 2005 with difference fields ($f_{123}-f_0$) in the left panels and ($f_{123}-f_0-\Delta f_l$) in the right panel. The outline of the urban area is included in black.

